Morphological stability analysis of directional solidification into an oscillatory fluid layer

Dmitri Volfson
School of Computational Science and Information Technology, Florida State University, Tallahassee, Florida 32306-4120

Jorge Viñals
School of Computational Science and Information Technology, Florida State University, Tallahassee, Florida 32306-4120
and Department of Chemical Engineering, FAMU-FSU College of Engineering, Tallahassee, Florida 31310-6046

(Received 17 April 2001; accepted 7 September 2001)

We study the stability of a planar solid-melt boundary during directional solidification of a binary alloy when the solid is being periodically vibrated in the direction parallel to the boundary (or equivalently, under a far field uniform and oscillatory flow parallel to the planar boundary). The analysis is motivated by directional solidification experiments under the low level residual acceleration field characteristic of a microgravity environment, and possible effects on crystal growth in space. It is known that periodic modulation of the solid-melt interface under the conditions stated induces second order stationary streaming flows within a boundary layer adjacent to the interface, the thickness of which is the same as the wavelength of the modulation. We derive an effective solute transport equation by averaging over the fast time scale of the oscillatory flow, and obtain the resulting dispersion relation for a small disturbance of a planar interface. We find both regions of stationary and oscillatory instability. For small ratios of the viscous to solutal layer thicknesses, s, the flow generally destabilizes the planar interface. For $s \simeq 1$, the flow stabilizes the stationary branch, but it can also excite an oscillatory instability. For large s, the effect of the flow is small. © *2001 American Institute of Physics.* [DOI: [10.1063/1.1416883]

I. INTRODUCTION

In a typical directional solidification experiment a sample is displaced at constant speed V within a furnace in which a prescribed temperature gradient is maintained. It is well known that a planar interface may become morphologically unstable,[1] and a great deal of research has addressed both this instability and the ensuing cellular steady states (see Refs. 2–5 for a review). It has also long been recognized that flow in the melt may have a pronounced effect on the stability of the interface.[6] In the case of a binary alloy, if the solute concentration of the solid and liquid phases is different, solute rejection or incorporation at the interface results in a density gradient that may cause thermosolutal convection in the melt. In addition, since the density of the solid phase is generally larger than that of the melt, conservation of mass requires fluid flow toward the interface. Given that the existing solute gradient ahead of the moving interface is the main driving force behind the morphological instability, flow in the melt that affects this solute distribution has a strong influence on the stability of the planar front.

Melt stirring is often used to reduce solute inhomogeneity, and to increase the stability of the planar interface. Delves[7] investigated solidification into a Blasius boundary layer and found that the interface may be stabilized for sufficiently fast stirring, and that, in contrast with the case without flow where the instability is stationary,[8] oscillatory modes bifurcate leading to traveling waves in the direction of the undisturbed plane parallel flow. However, interfacial perturbation modes with wave vectors perpendicular to the flow direction remain unaffected. Coriell *et al.*[9] considered solidification into a forced Couette flow, and showed that convective and morphological modes of instability are significantly decoupled. Interface perturbations with the wave vector parallel to the flow direction were found to be stabilized. The instability is oscillatory, and corresponds to traveling waves along the flow. Hobbs and Metzener performed an asymptotic analysis of long wavelength disturbances of the interface with a constant far field flow. They concluded that the additional solute transport caused by the flow has a destabilizing influence at small wave numbers, and that this flow induced destabilization is responsible for pattern selection.[10]

Brattkus and Davis[11,12] later studied the influence of nonparallel flows on the stability of the interface. They considered two configurations which are known to possess similarity solutions for the flow above the plane wall: stagnation point flow and von Kármán swirl flow.[13] In both cases, they showed that in the limit of large Schmidt number, and when the diffusive boundary layer is much thinner than the viscous layer, the interface is unstable to long wavelength perturbations with the unstable modes being traveling waves propagating against the flow direction. The nonparallel nature of the flow was found to be the destabilizing mechanism: The perpendicular flow component (toward the interface) compresses the solutal boundary layer and enhances instability, while the nonuniform parallel component induces horizontal

concentration gradients that lead to an oscillatory instability. Bühler and Davis,[14] and Chen and Davis[15,16] have considered the stability of an initially planar front solidifying into preexisting stationary and spatially periodic convective flows. When the lateral size of the roll-like convective cell is much larger than the critical wavelength for morphologically instability and the flow amplitude is weak, they find stationary instability modes that are localized near converging stagnation points. For sufficiently large sizes of the convective cell or large flow amplitude, the unstable modes are waves traveling from diverging to converging stagnation points, with amplitudes that are modulated with the same periodicity of the cellular structure.[14] The two-dimensional flow stabilizes two-dimensional disturbances of the interface, but destabilizes three-dimensional modes.[15] In the case of sufficiently strong three-dimensional flows, a variety of localized stationary interfacial patterns may be observed depending on the geometry of the stagnation regions of the flows.[16]

We finally mention a series of studies by Schulze and Davis[17–19] (see also the recent paper of Murray *et al.*[4]) devoted to the influence of time dependent shear flows on morphological stability. In Ref. 17 they considered a shear flow that is composed of steady and oscillatory components, the latter due to oscillation of the solid phase relative to the melt. A perturbation expansion in the ratio of the amplitude of the shear to the pulling speed shows that the flow ahead of the interface has periodic and stationary components, and that only the latter influences the instability threshold. Purely oscillatory shear flow enhances stability at all wave numbers within a range of frequencies. With a steady component added, the flow does not stabilize the small wave numbers as much as the purely oscillatory shear. They later addressed the case of a purely oscillatory shear, but with an elliptic polarization of the interface oscillation, still along its own plane.[18] They showed that perturbations of arbitrary wave vector couple to the flow if the phase lag θ between the two oscillatory components is not a multiple of π, with the coupling being largest for $\theta=\pi/2$. A numerical approach was then used to perform the linear stability analysis for finite values of the shear rate to pulling speed ratio. The results demonstrated the possibility of substantial or even complete suppression of the morphological instability with sufficiently strong shear.

The research that we describe here is an extension of that reported in Refs. 17–19, as our analytic approach is not restricted to small ratios of shear rate to pulling speed. We focus on the effect of an oscillatory planar flow on the morphological stability of an initially planar solidification front. Our study is based on the natural separation of time scales between the characteristic scale for the development of the instability near threshold, and the relaxation time of the oscillatory flow for a given instantaneous interfacial configuration. The base flow field for a planar interface has a Stokes layer structure, and does not alter the base solute distribution in the melt. A small perturbation of the interface induces a secondary nonplanar flow, which we calculate to first order in the amplitude of the interface perturbation. If the displacement of a fluid element far from the interface is small compared with the critical wavelength for morphological instability, the secondary flow has harmonic and steady components. At first order in the perturbation, only steady and harmonic components couple back to the interface perturbation. For the entire flow, including the steady part (also referred to as steady streaming), we adopt a quasi-static approximation according to which the flow relaxes instantaneously for any given configuration of the solid-melt interface. The steady streaming induces convection of the base solute distribution. In addition, the oscillatory part of the secondary flow also induces an oscillatory component of the concentration field, and its nonlinear interaction with the base oscillatory flow leads to additional mean solute transport. Both contributions modify the mean solute distribution and therefore the instability threshold. In Sec. II we briefly review the governing equations and the flow induced by periodic oscillation of a modulated solid boundary. We use this result to derive in Sec. III an effective solute transport equation and associated boundary conditions after averaging out all the oscillatory contributions. Section IV presents the results of a linear stability analysis of the equations and boundary conditions derived in Sec. III.

II. GOVERNING EQUATIONS AND BASE FLOW

We consider an initially planar solid–liquid interface in two spatial dimensions that is moving with constant speed V in the laboratory frame, and in the direction of the imposed temperature gradient. A co-moving system of coordinates is introduced such that $z=0$ is the average position of the interface, and the melt initially occupies the region $z>0$. A free stream velocity far ahead of the interface is prescribed which is oscillatory in time and parallel to the undisturbed interface. This may be accomplished in practice either by lateral oscillation of the solid with respect to the fluid, or by directly driving the oscillatory flow far from the solidifying front. In former case we would choose a system of coordinates rigidly attached to the oscillatory interface which would lead to the same system of equations after suitable definition of velocity and pressure. We also assume that the fluid is incompressible, and that gravity is absent, thus neglecting natural convection. Fluid motion is governed by the Navier–Stokes and continuity equations,

$$\partial_t \mathbf{u}+(\mathbf{u}\cdot\nabla)\mathbf{u}-V\,\partial_z\mathbf{u}=-\frac{\nabla p}{\rho}+\nu\Delta\mathbf{u}-a\omega^2\sin(\omega t)\mathbf{e}_x, \tag{1}$$

$$\nabla\cdot\mathbf{u}=0, \tag{2}$$

where $\mathbf{u}=(u,w)$ is the fluid velocity, p the pressure, ν the kinematic viscosity, and the far field fluid velocity is assumed periodic of angular frequency ω and amplitude a. Equations (1) and (2) have been written in the reference frame co-moving with the uniformly advancing average interface, but the velocity field is measured in the laboratory reference frame.

The boundary conditions are no-slip at the solid-melt interface,

$$\mathbf{u}\times\mathbf{n}=\mathbf{0} \quad \text{at} \quad z=\zeta(x,t), \tag{3}$$

where $\mathbf{n}$ is the unit normal to the interface directed toward the liquid. Neglecting intrinsic advection (caused by a density change upon solidification), we consider a solid–liquid interface that is impermeable,

$$\mathbf{u}\cdot\mathbf{n}=0 \quad \text{at} \quad z=\zeta(x,t). \tag{4}$$

The far field flow is defined by $\mathbf{u}=[a\omega\cos(\omega t),0]$ at $z=\infty$. We focus on the so-called one sided model of solidification.[2] The densities and thermal diffusivities of the solid and liquid phases are equal, latent heat produced at the interface is neglected, and diffusion in the solid is completely neglected. These assumptions allow one to decouple the temperature field from the velocity and solute fields, so that the temperature in both phases is a linear function of z, $T(z)=T_0+Gz$, where T_0 is the equilibrium melting temperature of a planar interface, and G is the constant temperature gradient. Solute transport is governed by the convection-diffusion equation,

$$\partial_t C+(\mathbf{u}\cdot\nabla)C-V\partial_z C=D\Delta C, \tag{5}$$

where C is the solute concentration in the liquid, and D the solute diffusivity in the liquid. Conservation of solute across the interface gives

$$D\,\mathbf{n}\cdot\nabla C=(K-1)C(\mathbf{u}_s\cdot\mathbf{n}) \quad \text{at} \quad z=\zeta(x,t), \tag{6}$$

where K is the segregation coefficient, defined as the ratio between the equilibrium solute concentrations in the solid and liquid, and $\mathbf{u}_s$ is the solidification velocity. The concentration at the interface is determined by the local temperature (according to the phase diagram), and modified by capillary effects (the Gibbs–Thomson equation),

$$T=T_M+mC-T_M\frac{\gamma}{L_v}\mathcal{K}, \tag{7}$$

where T_M is the equilibrium melting temperature of the pure substance, m is the slope of the liquidus line, γ is the interfacial free energy per unit surface, L_v is latent heat per unit volume, and $\mathcal{K}$ is the mean curvature of the interface defined positive for a sphere.

We recast the Navier–Stokes and continuity equations (1) and (2) in dimensionless form by using a stream function formulation,

$$\partial_t\Delta\psi+\mathrm{Re}\frac{\partial(\psi,\Delta\psi)}{\partial(z,x)}-\frac{s}{Sc}\partial_z\Delta\psi=\Delta^2\psi, \tag{8}$$

where the stream function ψ is such that $\mathbf{u}=(\partial_z\psi,-\partial_x\psi)$. We have made lengths dimensionless by δ_s, the stream function by $a\omega\delta_s$, time by $1/\omega$, and introduced the Reynolds number $\mathrm{Re}=a/\delta_s$, and the ratio $s=\delta_s/\delta$ between the Stokes layer thickness $\delta_s=\sqrt{\nu/\omega}$ and the solutal layer thickness $\delta=D/V$. $\mathrm{Sc}=\nu/D$ is the Schmidt number. We have also used the notation $\partial(a,b)/\partial(z,x)=(\partial_z a)(\partial_x b)-(\partial_x a)(\partial_z b)$ for the nonlinear term. In what follows, we assume that s is finite, and that Sc is large [we will neglect terms of order $\mathcal{O}(\mathrm{Sc}^{-1})$ and higher]. These assumptions are not restrictive. For example, for a Pb–Sn alloy $\mathrm{Sc}=81.0$, and for pulling speeds in the range $V\sim 10-100\,\mu$m, and frequency in the range $\omega\sim 10^1-10^3\ \mathrm{s}^{-1}$ we have $s\sim 5.2\times10^{-2}-10^0$ (material parameters for typical experimental conditions may be found in Ref. 20).

Since the far free-stream flow is parallel to the undisturbed interface at $z=0$, the base flow does not affect the base solute distribution, as both depend only on z. Only perturbations of the base flow field and of the base solute distribution induced by interface perturbations couple. The linear stability analysis will consider interfacial perturbations of the form $z=\epsilon\zeta(x)=\epsilon e^{ikx}$, where $\epsilon=\zeta^*/\delta_s$ is the dimensionless amplitude of the perturbation and $k=2\pi\delta_s/\lambda$ is its wave number. The stability analysis that we present is restricted to the quasi-static approximation in which velocity field in the bulk fluid instantaneously relaxes for any given configuration of the interface. We therefore first solve for the flow field given a fixed interfacial configuration, then average the solute transport equation and boundary conditions to incorporate the effect of the secondary nonplanar component of the velocity field, and use the resulting equation to analyze the morphological stability of the interface.

For a given interfacial configuration, the flow field in the melt satisfies

$$\partial_t\Delta\psi+\mathrm{Re}\frac{\partial(\psi,\Delta\psi)}{\partial(z,x)}=\Delta^2\psi, \tag{9}$$

with no-slip conditions at the boundary, and we have neglected terms of the order of s/Sc, $\psi=\partial_z\psi=0$ at $z=\epsilon\zeta$, and $\partial_x\psi=0$, $\partial_z\psi=\frac{1}{2}e^{it}+\text{c.c.}$ at $z=\infty$. The stream function ψ and the boundary conditions are first expanded in power series of ϵ, $\psi=\psi_0+\epsilon\psi_1+\cdots$, $\psi(z)|_{z=\epsilon\zeta}=\psi_0(z)|_{z=0}+\epsilon(\psi_1(z)|_{z=0}+\zeta\partial_z\psi_0(z)|_{z=0})+\cdots$, and the solution found order by order in ϵ. At zeroth order the interface is effectively planar and the flow is a transverse wave, the so-called Stokes layer,

$$\tilde{u}_0=\partial_z\psi_0(z,t)=\frac{e^{it}}{2}\hat{u}_0(z)+\text{c.c.}, \quad \hat{u}_0(z)=1-e^{-\alpha z}, \tag{10}$$

where $\alpha=(1+i)/\sqrt{2}$. In the following, a tilde over a variable will denote its oscillatory component, and a bar its average over the fast time scale. At first order in ϵ one has the Orr–Sommerfeld equation with inhomogeneous boundary conditions. The equation can be solved perturbatively in the limit $k\,\mathrm{Re}=2\pi a/\lambda\ll 1$ by expanding the amplitude $\psi_1(z,t)$ in power series of $k\,\mathrm{Re}$. One finds

$$\psi_1=\overline{\psi_1}+\tilde{\psi}_1+HFT+\mathcal{O}((k\,\mathrm{Re})^2), \tag{11}$$

$$\tilde{\psi}_1=e^{ikx}\left[\frac{e^{it}}{2}\hat{\phi}_0(z)+\text{c.c.}\right],$$
$$\hat{\phi}_0(z)=\frac{\alpha}{\rho-k}(e^{-\rho z}-e^{-kz}), \tag{12}$$

$$\overline{\psi_1}=ik\,\mathrm{Re}\,e^{ikx}[\hat{\chi}_0(z)+\text{c.c.}],$$
$$\hat{\chi}_0(z)=\frac{\alpha^3}{4(\rho-k)}(A_1e^{-\rho z}+A_2e^{-(\rho+\alpha^*)z}+A_3e^{-(k+\alpha^*)z} \tag{13}$$
$$+(B_1+B_2z)e^{-kz}),$$

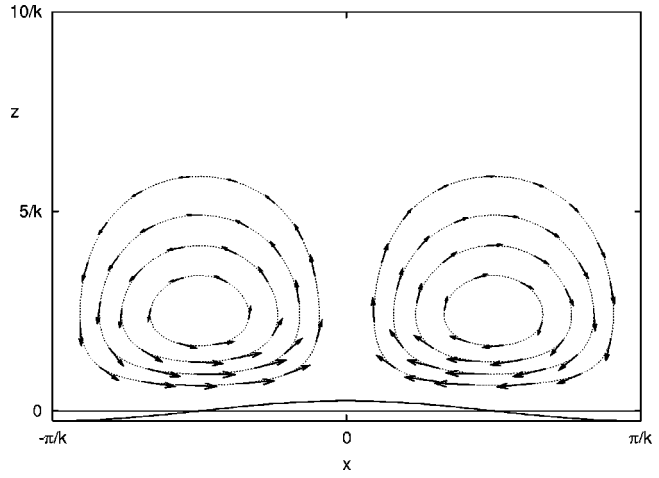

FIG. 1. Sketch of the streamlines and velocity field of the steady streaming over a modulated boundary $z=\epsilon\cos(kx)$ of large wave number $k=2\pi\delta_s/\lambda\gg1$. The flow is comprised of two recirculating cells per wall period. The amplitude of the boundary profile (bold solid line) has been magnified for clarity.

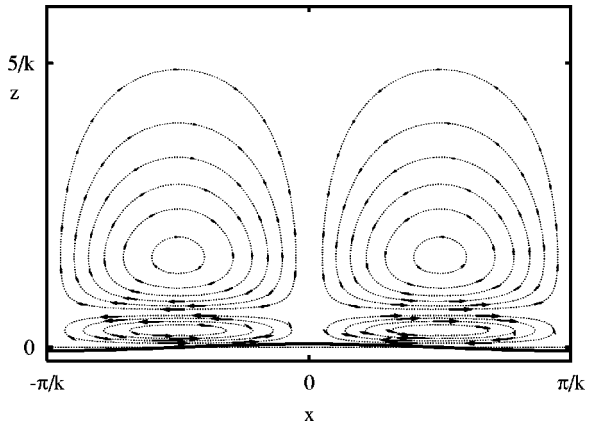

FIG. 2. Sketch of the streamlines and velocity field of the steady streaming over a modulated boundary $z=\epsilon\cos(kx)$ of small wave number $2\pi\delta_s/\lambda\ll1$. The flow is comprised of two pairs of recirculating cells per wall period, with the fluid rotating in opposite directions. The amplitude of the boundary profile (bold solid line) has been magnified for clarity.

$$\tilde{u}_1=\partial_z\tilde{\psi}_1,\quad \overline{u}_1=\partial_z\overline{\psi}_1,\quad \tilde{w}_1=-\partial_x\tilde{\psi}_1,\quad \overline{w}_1=-\partial_x\overline{\psi}_1, \tag{14}$$

where $\rho=(i+k^2)^{1/2}$ with $\Re\{\rho\}>0$ so as to have bounded solutions as $z\to\infty$, and the coefficients $A_{i=1,2,3}$ and $B_{i=1,2}$ are given in the Appendix; HFT stands for higher harmonic flow components which only contribute higher order corrections to the morphological stability analysis of Sec. IV, and are therefore neglected. In Eq. (13) the field $\hat{\chi}$ obtained as an $\mathcal{O}(k\,\mathrm{Re})$ correction to periodic component $\tilde{\psi}_1$ describes the time independent part of the secondary flow, the so-called steady streaming. The solution given by Eqs. (10)–(12) was first given in Ref. 21, and further discussed and extended to random vibration in Ref. 22. We summarize here its salient qualitative features. When the Stokes layer thickness is larger than the interface wavelength ($k\gg1$), the boundary layer is confined to the region $z\lesssim1/k$. Steady cellular flow is obtained ahead of the perturbed interface, with two recirculating cells per wavelength (see Fig. 1). The normal component of the velocity is in phase with the interfacial distortion, so it is largest and directed toward the fluid ahead of the crests of the interface. When the thickness of the Stokes layer is smaller than wavelength $k\ll1$, the boundary layer has four recirculating cells per wavelength (see Fig. 2). Two cells are adjacent to the interface with a recirculation direction that is the same as in the limit $k\gg1$, and they extend over a distance of the order of the Stokes layer thickness. The second pair of cells stack on top of the other two, and the fluid rotates in the opposite direction. The flow extends up to distances of the order of $z\sim1/k$.

We confine our study to the case in which the amplitude of oscillation of the fluid elements far from the interface is much smaller than the boundary wavelength ($2\pi a/\lambda\ll1$). The opposite limit of $k\,\mathrm{Re}\gg1$ could be considered analytically as well but it would be necessary to address the stability of the flow itself. We wish to avoid this complication and to remain within the region of applicability of the quasi-static approximation for the flow.

III. EFFECTIVE SOLUTE TRANSPORT ABOVE AN OSCILLATORY, MODULATED BOUNDARY

In this section, we use the flow field described in Sec. II to derive an effective solute transport equation that is valid in the slow time scale associated with the morphological instability. We redefine time and length scales from those given in Sec. II: the time scale from $1/\omega$ to D/V^2 (so that $t\to\Omega t$, with $\Omega=\omega D/V^2$), and the length scale from δ_s to $\delta=D/V$, (so that $(x,z)\to(x,z)/s$), and hence $k\to ks$ and $\epsilon\to\hat{\zeta}/s$. The velocity scale is changed from $a\omega$ to V [so that $(u,w)\to a\omega/V(u,w)$]. We restrict our analysis to the case in which the ratio of the Stokes layer thickness to the solutal layer thickness s is finite. Since $\Omega=\mathrm{Sc}/s^2$, the assumptions already introduced imply that Ω is of the same order as the Schmidt number. We also note that $a\omega/V=\mathrm{Re}\,\mathrm{Sc}/s$, so that this group may be small compared to Sc ($k\,\mathrm{Re}\ll1$), but larger than $\mathcal{O}(1)$. The equation for solute transport and associated boundary conditions in dimensionless form are

$$\partial_t C+\frac{\mathrm{Re}\,\mathrm{Sc}}{s}(\mathbf{u}\cdot\nabla C)=\partial_z C+\Delta C, \tag{15}$$

and

$$(1+\partial_t\zeta)[K+(1-K)C]=-\partial_z C+\partial_x\zeta\,\partial_x C, \tag{16}$$

$$C-1+M^{-1}\zeta+\Gamma\mathcal{K}=0, \tag{17}$$

at $z=\zeta(x,t)$. Concentration has been scaled by $\Delta C_0=C_\infty/K-C_\infty$, so that the dimensional concentration $C^*=C_\infty+\Delta C_0 C$. We have also introduced the dimensionless inverse morphological number $M^{-1}=-G\delta/m\Delta C_0$, and the surface energy parameter $\Gamma=-T_M\gamma/\delta m\Delta C_0 L_v$. The morphological number represents the degree of constitutional supercooling, and is proportional to the gradient of concentration $\Delta C_0/\delta$ that builds up ahead of a planar interface moving with speed V.

The base solution corresponds to a planar front, an exponential solute profile, and a planar and parallel oscillatory flow

$$\zeta_0=0, \quad C_0=e^{-z}, \quad \mathbf{u}_0=(\tilde{u}_0(z/s,\Omega t),0), \tag{18}$$

where $\tilde{u}_0$ is given by Eq. (10). We next consider a time dependent interface perturbation $\zeta=\zeta_1(x,t)=\hat{\zeta}e^{ikx+\sigma t}$, and write the corresponding perturbations for solute and velocity fields: $C=C_0+C_1(x,z,t)$, $\mathbf{u}=\mathbf{u}_0+\mathbf{u}_1(x/s,z/s,\Omega t)$, where all the perturbations are assumed of the same order, and the components of $\mathbf{u}_1=s^{-1}\hat{\zeta}(\tilde{u}_1+\overline{u_1},\tilde{w}_1+\overline{w_1})$ are given by Eqs. (11)–(13). Since the nonlinear term in Eq. (15) contains a velocity field that is comprised of oscillatory and mean parts, a similar decomposition will hold for the concentration field. We apply the method of multiple time scales and split the time derivative and the concentration field into oscillatory and slowly varying parts: $\partial_t=\Omega\partial_\tau+\partial_t$, $C_1=\tilde{C}_1(\tau)+\overline{C_1}(t)$, where $\tau=\Omega t$ is the fast time. With this decomposition Eq. (15) leads to

$$\Omega\partial_\tau\tilde{C}_1+\frac{\mathrm{Re\,Sc}}{s}\left[\tilde{u}_0\,\partial_x\overline{C_1}+\frac{\hat{\zeta}}{s}C_0'\tilde{w}_1+\{\tilde{u}_0\,\partial_x\tilde{C}_1\}\right]=\partial_z\tilde{C}_1+\Delta\tilde{C}_1, \tag{19}$$

$$\partial_t\overline{C_1}+\frac{\mathrm{Re\,Sc}}{s}\left[\langle\tilde{u}_0\,\partial_x\tilde{C}_1\rangle+\frac{\hat{\zeta}}{s}C_0'\overline{w_1}\right]=\partial_z\overline{C_1}+\Delta\overline{C_1}, \tag{20}$$

where $C_0'=dC_0/dz$, and the oscillatory components are functions of the fast time $\tau=\Omega t$, with zero mean over the fast time scale (averaging over the fast time scale is denoted by $\langle\cdot\rangle$; $\{\cdot\}$ on the other hand, stands for the oscillatory component of a quantity).

Fast oscillatory dynamics does not directly couple to the interface perturbation; instead it induces solute redistribution on the slow time scale which then affects the stability of the interface. The solution for the mean part of the solute perturbation $\overline{C_1}$ follows from Eq. (20), where the only term that couples to the fast solute dynamics of Eq. (19) is $\langle\tilde{u}_0\,\partial_x\tilde{C}_1\rangle$. Furthermore, we only need the harmonic response component of $\tilde{C}_1$ (at frequency Ω). Since nonlinear terms in Eq. (19) are proportional to Sc, and thus dominant compared to all other terms in the right hand side, we write

$$\Omega\,\partial_\tau\tilde{C}_1+\frac{\mathrm{Re\,Sc}}{s}\left[\tilde{u}_0\,\partial_x\overline{C_1}+\frac{\hat{\zeta}}{s}C_0'\tilde{w}_1+\{\tilde{u}_0\,\partial_x\tilde{C}_1\}\right]=0. \tag{21}$$

The third term within brackets in Eq. (21) can lead to harmonic response of $\tilde{C}_1$ only through interaction between $\tilde{u}_0$ and $\tilde{C}_1$ of the form $\tilde{C}_1\propto e^{\pm 2i\Omega t}$, a term that is proportional to $\mathrm{Re}\,k\ll 1$, and hence small compared with the two other convective terms in Eq. (21). Thus it can be dropped out consistent with our approximation for the Navier–Stokes equation which neglects terms of order $\mathcal{O}(\mathrm{Re}^2k^2)$. The first term within brackets in Eq. (21) does not contribute to $\langle\tilde{u}_0\,\partial_x\tilde{C}_1\rangle$ because $\tilde{C}_1$ is now out of phase with $\tilde{u}_0$. In order to show this, define $\tilde{\Phi}=\Omega^{-1}\int\tilde{u}_0\,d\tau$, an Eulerian displacement field. We now have $\tilde{C}_1=-\mathrm{Re}\,s\,\tilde{\Phi}\,\partial_x\overline{C_1}+\cdots$, where the dots stand for slowly varying terms. Then $\langle\tilde{u}_0\,\partial_x\tilde{C}_1\rangle=-\mathrm{Re}\,s\,\langle\tilde{u}_0\tilde{\Phi}\rangle\partial_x^2\overline{C_1}=-\mathrm{Re}\,s\,\Omega\langle\tilde{\Phi}\,\partial_\tau\tilde{\Phi}\rangle\partial_x^2\overline{C_1}=0$. Therefore, only the second term within brackets in Eq. (21) remains as a contribution to the calculation of $\tilde{C}_1$. Integration of this term yields

$$\tilde{C}_1=-\mathrm{Re}\,C_0'\hat{\zeta}\int\tilde{w}_1\,d\tau+\cdots, \tag{22}$$

where we used $\mathrm{Sc}=\Omega s^2$ and $\cdots$ stand for slowly varying terms that do not contribute to the average transport of solute within our approximation. Substituting the explicit expressions from Eqs. (22), (12), and (13), we find that the average transport which is induced by nonlinear interaction between the base oscillatory velocity field and the oscillatory component of the solute perturbation is

$$\frac{\mathrm{Re\,Sc}}{s}\langle\tilde{u}_0\,\partial_x\tilde{C}_1\rangle=-k^2\mu C_0'\hat{\zeta}e^{ikx}\left[\frac{\hat{u}_0^*\hat{\phi}_0}{4i}+\mathrm{c.c.}\right], \tag{23}$$

where $\mu=\mathrm{Re}^2\,\mathrm{Sc}=a^2\omega/D$ is a dimensionless group which we assume to be finite (this requires $\mathrm{Re}\propto 1/\sqrt{\mathrm{Sc}}$).

Similarly, using again Eqs. (12) and (13), we find the second mean transport term in Eq. (20),

$$\frac{\mathrm{Re\,Sc}}{s^2}\hat{\zeta}C_0'\overline{w_1}=k^2\mu C_0'\hat{\zeta}e^{ikx}[\hat{\chi}+\mathrm{c.c.}]. \tag{24}$$

Since both Eqs. (23) and (24) are of the same order, and have a similar spatial structure, it is convenient to combine them into one single field defined as

$$\frac{\mathrm{Re\,Sc}}{s}\left[\langle\tilde{u}_0\,\partial_x\tilde{C}_1\rangle+\frac{\hat{\zeta}}{s}C_0'\tilde{w}_1\right]=k^2\mu C_0'\hat{\zeta}\,e^{ikx}[\,\hat{\pi}+\mathrm{c.c.}], \tag{25}$$

where

$$\hat{\pi}=\frac{\alpha^3}{4(\rho_s-ks)}[E_1e^{-(\rho_s+\alpha^*)z/s}+E_2e^{-(ks+\alpha^*)z/s}+(F_1+F_2z/s)e^{-kz}], \tag{26}$$

where $\rho_s=\sqrt{k^2s^2+i}$, $\Re\{\rho_s\}>0$, and the coefficients E_1, E_2, F_1, F_2 are given in the Appendix. Note that, by construction, $\hat{\pi}=\hat{\pi}'=0$ at $z=0$. Equations (20), (25), and (26) are the main results of this section.

We next consider the decomposition of the boundary conditions into oscillatory and mean parts. The oscillatory components of Eqs. (16) and (17) yield $\tilde{C}_1=\partial_z\tilde{C}_1=0$. It is easy to see from Eq. (22) that the condition $\tilde{C}_1=0$ is automatically satisfied because $\tilde{w}_1(z=0)=0$, but the condition $\partial_z\tilde{C}_1=0$ is not. Recall that $\tilde{C}_1$ was obtained from Eq. (19) by neglecting the right hand side. Thus we have formally reduced the order of the differential equation from two to zero. As a consequence, we cannot impose any boundary conditions on $\tilde{C}_1$, and the fact that one is satisfied is accidental. In order to properly take into account both boundary conditions on $\tilde{C}_1$ in the limit $\Omega\propto\mathrm{Sc}\gg 1$, one needs to introduce a matched expansion involving a boundary layer of thickness $\mathcal{O}(\mathrm{Sc}^{-1/2})$ in the vicinity of the interface. However, this procedure will only lead to small corrections under the assumption that $\mathrm{Sc}\gg 1$. The situation is similar to that considered by Wheeler *et al.*,[23] who studied the onset of so-

lutal convection in directional solidification (with a nondeformable solid–liquid interface) when the system is subjected to high frequency vertical vibration. As is the case in our study, the leading order solution in their case is the outer solution and it does not satisfy the interfacial boundary conditions.

Averaging the boundary conditions Eqs. (16) and (17) over the fast time scale we find,

$$(1+\partial_t\zeta)[K+(1-K)\overline{C}]=-\partial_z\overline{C}+\partial_x\zeta\,\partial_x\overline{C}, \tag{27}$$

$$\overline{C}-1+M^{-1}\zeta+\Gamma\mathcal{K}=0, \tag{28}$$

both at $z=\zeta(x,t)$.

In the following section, we study the stability of a planar interface given the averaged solute transport equation (20), supplemented by Eq. (25) and Eq. (26), with boundary conditions (27) and (28).

IV. LINEAR STABILITY ANALYSIS

We study the linear stability of a planar interface when solute transport by mean flow is taken into account. We assume a solution of the form,

$$\overline{C}=C_0+e^{ikx+\sigma t}\{\hat{\overline{C}}_1e^{-qz}+\hat{\zeta}\mu k^2h(z)\}, \tag{29}$$

where σ is the growth rate, the branch $\mathcal{R}(q)>0$ for $q=1/2+1/2\sqrt{1+4(\sigma+k^2)}$ is chosen so that perturbations decay at infinity, and a field $h(z)$ is introduced to incorporate the inhomogeneity due to the mean transport. Substitution of Eq. (29) into Eq. (20) yields the following equation for $h(z)$

$$h''+h'-(\sigma+k^2)h=C_0'[\pi+\text{c.c.}]. \tag{30}$$

Note that for a linear analysis we only need the values $h_0=h(z;\sigma,k,s)|_{z=0}$ and $g_0=dh(z;\sigma,k,s)/dz|_{z=0}$ computed for a particular solution of Eq. (30). They are given in the Appendix. The functions $h_0(\sigma,k,s)$ and $g_0(\sigma,k,s)$ are real provided that σ is real, and complex otherwise.

By linearizing the boundary conditions (27) and (28) about the base solution (18), we arrive at an eigenvalue problem for the growth rate σ. The requirement that there be nontrivial solutions to the perturbation equations leads to a dispersion relation given by

$$\sigma+K=[K+q-1][1-M^{-1}-\Gamma k^2]-\mu k^2[qh_0+g_0]. \tag{31}$$

Equation (31) is the main result of this paper. In the absence of flow ($\mu=0$), the classical dispersion relation for the one-sided model of solidification is recovered.[2]

Some general features of the dispersion relation are the following: Uniform perturbations ($k=0$) are damped ($\sigma=-KM^{-1}$) unless $M^{-1}=0$ or $K=0$. The $k=0$ mode is an infinitesimal translation of the planar front toward higher temperatures where it melts back. Furthermore, this mode does not induce any normal flow. Flow in the melt breaks reflection symmetry ($x\to-x$), and hence Eq. (31) is no longer invariant under $k\to-k$. On the stationary instability branch, regions with positive perturbations of the concentration h_0 and of the concentration gradient g_0 stabilize the planar interface. The first observation follows from the associated decrease in the local melting temperature, whereas the second is related to a decrease in the magnitude of the destabilizing concentration gradient ahead of the interface. The quantity k^2qh_0 is positive at small k, and negative at large k. Therefore its contribution to the concentration perturbation is stabilizing at small k, and destabilizing at large k. The contribution from the term k^2g_0 shows exactly the opposite trend. In fact, both terms very nearly cancel for large and small k, so that the effect of the flow is most pronounced at finite wave numbers.

It is useful to start the analysis of the dispersion relation Eq. (31) by presenting analytical results that can be obtained in the long wavelength limit. For $k\ll1$ we find a stationary branch given by

$$M^{-1}=-\Gamma k^2+\frac{k^2}{K}-\frac{1+K}{K^2}k^4+\mu k^3\frac{f_1(s)}{K}+\mu k^4\frac{f_2(s)}{K}+\mathcal{O}(k^5), \tag{32}$$

and the functions $f_{1,2}(s)$ are given in the Appendix. To lowest order in k, the neutral stability curve is not affected by the flow. The first contribution arising from the flow appears at $\mathcal{O}(\mu k^3)$, and can be stabilizing or destabilizing since the function $f_1(s)$ is negative for $0\leqslant s<s^*$ and positive for $s^*\leqslant s<\infty$ ($s^*=(\sqrt{14}-\sqrt{2})/2\approx1.16$). Therefore, the cubic term is stabilizing for $s<s^*$, and destabilizing otherwise. Note that increasing the dimensional angular frequency ω results in larger values of $\mu\propto\omega$, but smaller values of the ratio $s\propto\omega^{-1/2}$. Sufficiently strong driving, which is necessary for appreciable stabilization, may be achieved without significant compression of the Stokes layer. Alternatively, an increase of the forcing strength may be accomplished with a small increase of the driving amplitude ($\mu\sim a^2$), while keeping ω fixed. However, the applicability of the latter approach is limited by the assumption $2\pi a/\lambda\ll1$, that may be rewritten as $sk\sqrt{\mu/Sc}\ll1$. To ensure the self-consistency of our approach the wave numbers of the most unstable perturbation must satisfy this inequality for given values of μ and Sc. The restriction on μ is not severe as the Schmidt number is assumed to be large. Finally $f_2(s)$ is always negative (and bounded between $-3/2$ and -2.615). Thus the term $\mathcal{O}(\mu k^4)$ is always stabilizing.

These results may be compared with those of Schulze and Davis[18,19] who derived an analytic expression for the neutral stability curve in the long wavelength ($k\to0$) and small shear ($a\omega/V\to0$) limit. They also studied numerically the stability under arbitrary wave numbers and shears. Our analytical results complement theirs in that we obtain an analytical form of the dispersion relation for arbitrary wave numbers and shear rates, but under a different set of approximations ($\text{Sc}\sim\Omega\gg1, a\ll\lambda$). Even though a is small, the fact that we allow large frequencies implies that our calculation is not restricted to small shear rates (note the $\sqrt{\mu\Omega}=a\omega/V$, the latter being the expansion parameter used in Ref. 18).

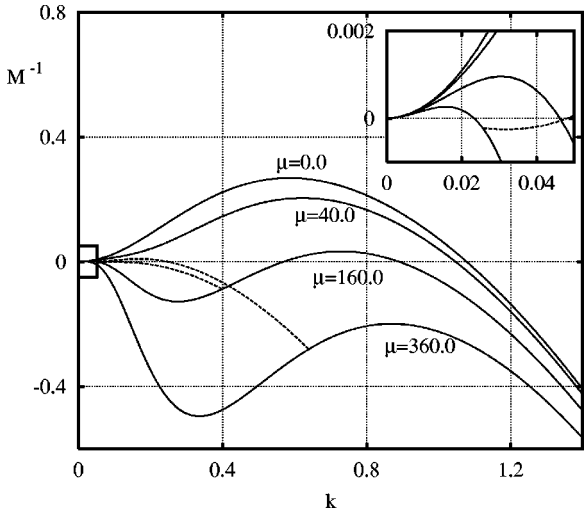

FIG. 3. Neutral curves $M^{-1}(k)$ for stationary (solid lines) and oscillatory (dashed lines) instability for $K=0.3$, $s=2.85$, $\Gamma=0.6$, and a set of values of μ. The inset shows the region near the origin, and that the long wavelength instability is not completely suppressed even for large $\mu=360$.

In Ref. 19 Schulze and Davis derived a nonlinear and long wave evolution equation in the limit of small $a\omega/V$ and near the absolute stability limit. The linearized form of their evolution equation gave the neutral stability curve, which is in good agreement with ours not only for $\Omega\,\mathrm{Sc}\gg 1$ but even for $\Omega\,\mathrm{Sc}\sim 1$. In particular, they found a curve in the (Sc,Ω) plane separating the regions for which the flow is stabilizing or destabilizing at large wavelengths. This curve is well approximated by the function $\Omega\approx 0.73\,\mathrm{Sc}+4.7$, starting from fairly small values of $\mathrm{Sc}>1$. We find $\Omega\sim 0.738\,\mathrm{Sc}$ assuming that $\mathrm{Sc}\sim\Omega\gg 1$ (recall that $s=\sqrt{\mathrm{Sc}/\Omega}$, and we use the value of $s^*\simeq 1.16$ given above that gives the boundary between regions in which the flow is stabilizing or destabilizing). Hence, we find that our asymptotic approximation holds, at least for the long wavelength disturbances, from surprisingly small values Schmidt number and dimensionless frequency. Note that it also holds for large values of $a\omega/V$ where, for example, the numerical approach of Ref. 18 fails because of computational complexity.

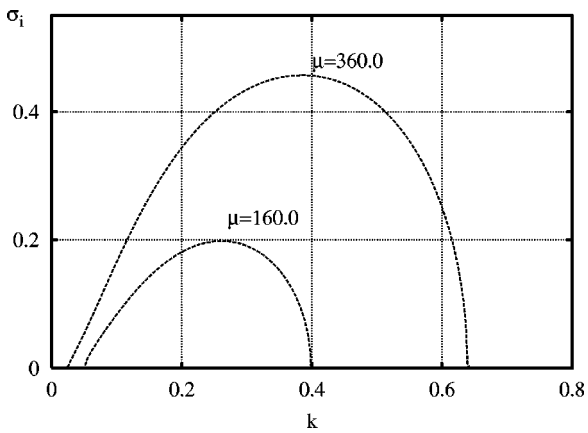

FIG. 4. The positive Hopf frequency σ_i as a function of the wave number k corresponding to the oscillatory branches of the neutral curves of Fig. 3 above for two different values of μ.

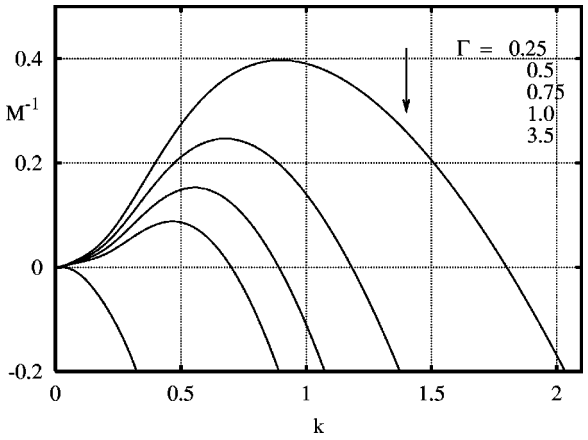

FIG. 5. Neutral curves $M^{-1}(k)$ for stationary (solid lines) and oscillatory (dashed lines) instability for $K=0.3$, $s=2.85$, $\mu=40.0$, and a set of values of Γ.

We first compare the neutral curves obtained from Eq. (31) and the numerical linear stability analysis of Eqs. (15)–(17) given in Ref. 18. Their study considered the following set of parameters: $K=0.3$, $\Gamma=0.6$, $\mathrm{Sc}=81.0$, $\Omega=10$, and a number of values of $a\omega/V$. In Fig. 3 we show our results for the neutral curves for a set of parameters that corresponds to Fig. 4 in Ref. 18 ($K=0.3$, $\Gamma=0.6$, $s=2.85$, and $\mu=0, 40, 160, 360$). The agreement is good for small to moderate values of μ, but it becomes worse with increasing μ. The solutal layer thickness is of the same order as Stokes layer thickness, and the flow tends to stabilize long wavelength perturbations. We find that long wavelength modes are always unstable (inset of the Fig. 3) though the range of instability narrows as μ is increased. As discussed in the previous section, the flow has no influence on perturbations of sufficiently small wave numbers. A new feature of our results is the appearance of an oscillatory (Hopf) instability for sufficiency large values of μ and at finite wave numbers, leading to a discontinuity in $k_c(\mu)$, the critical wave number for instability. Figure 4 shows the dependence of the Hopf frequency on the wave number.

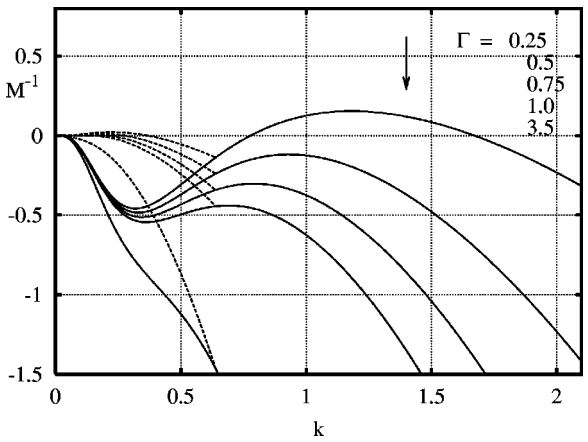

FIG. 6. Neutral curves $M^{-1}(k)$ for stationary (solid lines) and oscillatory (dashed lines) instability for $K=0.3$, $s=2.85$, $\mu=360.0$, and a set of values of Γ.

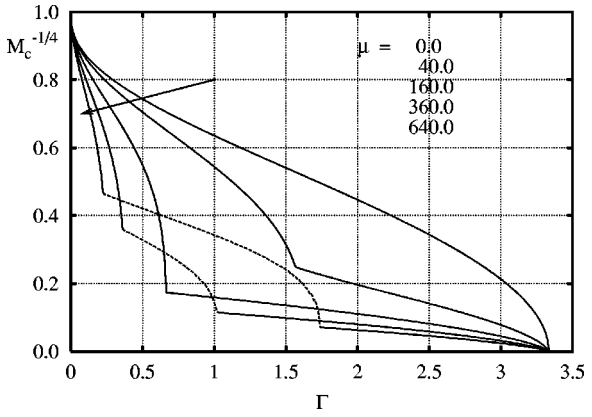

FIG. 7. Critical curves $M_c^{-1}(\Gamma)$ (from the maxima of the corresponding neutral curves) for stationary (solid lines) and oscillatory (dashed lines) instability for $K=0.3$, $s=2.85$, and a set of values of μ.

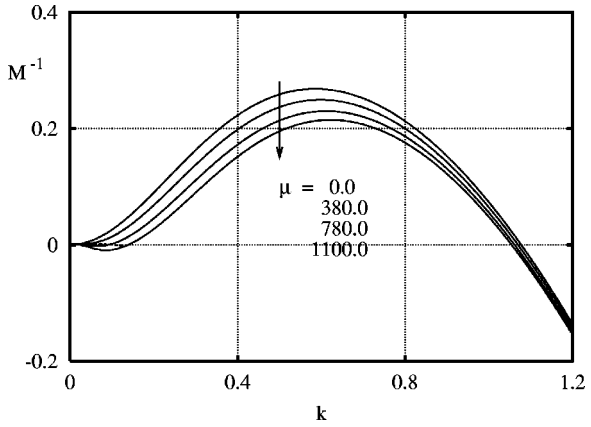

FIG. 9. Neutral curves $M^{-1}(k)$ for stationary (solid lines) and oscillatory (dashed lines) instability for $K=0.3$, $s=10.0$, $\Gamma=0.6$, and a set of values of μ.

We next present additional cuts of the neutral surface. Figures 5 and 6 show the neutral curves as the surface energy parameter Γ is increased from small values toward the absolute stability limit ($\Gamma=1/K$ in the absence of flow). Figure 5 shows the case $\mu=40$ in which the oscillatory instability does not appear, and Fig. 6 shows the corresponding curve for $\mu=360$, including an oscillatory branch. Figures 7 and 8 show the resulting dependence of the critical morphological number and critical wave number, respectively, as a function of Γ. At sufficiently low values of μ, the instability is stationary (Fig. 5), and flow generally acts to stabilize the planar interface (Fig. 7). Within this range, two types of instability may occur at either a finite or low wave number, depending on the value of Γ (the transition between them is marked by the appearance of a cusp in Fig. 7, and a discontinuity in Fig. 8). At yet higher values of μ, an additional oscillatory branch appears between the finite and low wave number stationary branches (dashed lines in Figs. 6–8). As stated above, our results for $s=2.85$ generally agree with those of Schulze and Davis,[18] except in that they report a complete suppression of the instability for sufficiently large values of $a\omega/V$, and in that they do not observe the oscillatory instability.

We now turn to the case $s=10.0$ in which the Stokes layer thickness is much larger than the solutal layer thickness. In this limit, the solutal layer is not appreciably modified by the flow, and hence the morphological stability boundaries depend only weakly on the flow. The neutral curves for $K=0.3$, $\Gamma=0.6$ and a range of values of μ are shown in Fig. 9. The effect of the flow is now very small because the streaming flow is very weak near the interface, and hence the redistribution of solute by the flow near the interface is weak as well.

In the opposite limit of small s, the Stokes layer thickness is small compared with the solutal layer thickness, and flow significantly changes the morphological instability threshold. We present in Fig. 10 the neutral stability curves for $s=0.1$, $K=0.3$, and $\Gamma=0.6$, and in Fig. 11 its dependence on Γ. The corresponding critical curves are shown in Figs. 12 and 13 for a range of values of μ. Figure 10 shows that flow can, in fact, destabilize the interface, but only at finite wave numbers. A separate analysis of qh_0 and g_0 in Eq. (31) reveals that while the shift in the concentration at the interface that is induced by the flow has a stabilizing

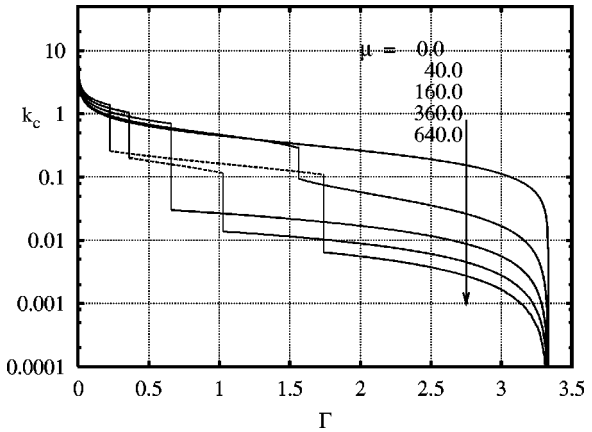

FIG. 8. Values of the critical wave number k_c as a function of Γ of stationary (solid lines) and oscillatory (dashed lines) instabilities for $K=0.3$, $s=2.85$, and a set of values of μ.

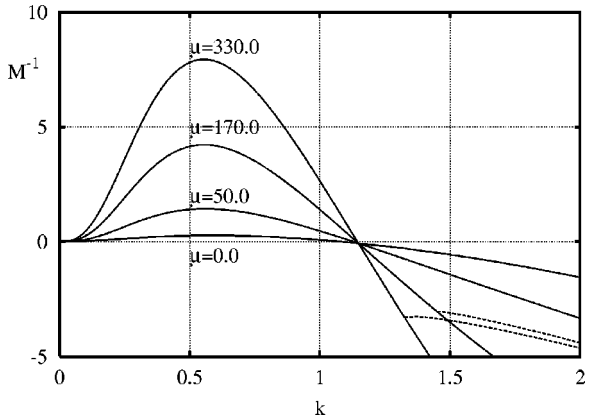

FIG. 10. Neutral curves $M^{-1}(k)$ for stationary (solid lines) and oscillatory (dashed lines) instability for $K=0.3$, $s=0.1$, $\Gamma=0.6$, and a set of values of μ.

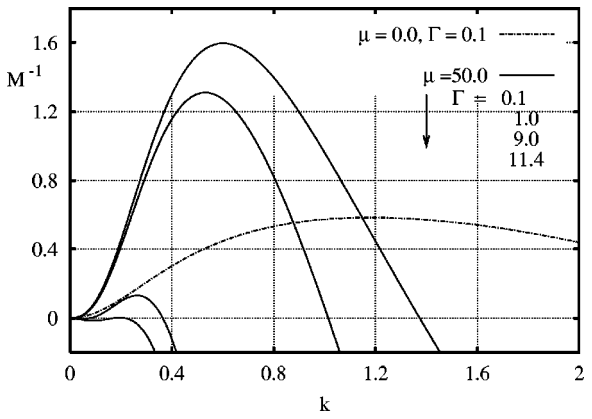

FIG. 11. Neutral curves $M^{-1}(k)$ for $K=0.3$, $s=0.1$, and $\mu=50.0$ and several values of Γ (solid lines). As a reference we also plot the neutral curve of the no flow case ($\mu=0$) for $K=0.3$ and $\Gamma=0.1$.

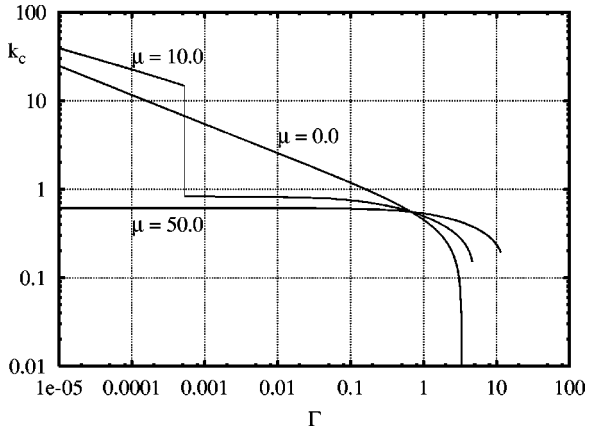

FIG. 13. Values of the critical wave number k_c as a function of Γ for $K=0.3$, $s=0.1$, and a set of values of μ.

effect, there is also an increase in the magnitude of the concentration gradient that promotes instability. Note that the instability persists beyond the absolute stability limit in the case without flow, as shown in Fig. 12. Figure 13 shows the corresponding values of k_c. The curve $k_c(\Gamma)$ at large Γ terminates at a finite value of k_c, in contrast with the no flow case where $k_c \to 0$ as the absolute stability limit is approached.

As an example, we present the stability diagram computed from Eq. (31) with material parameters appropriate for the binary succinonitrile-acetone grown in a temperature gradient of $G=20\,\mathrm{K/cm}$.[24] The Schmidt number of this alloy is large ($\mathrm{Sc}=2050$), and hence our quasi-static approximation for the flow is expected to hold. We consider pulling speed V, melt concentration away from the interface C_∞, flow angular frequency ω and amplitude a as experimentally adjustable parameters. For fixed a, ω, and V the neutral curve $C_\infty(\lambda)$ always has at least one minimum for a critical wavelength λ_c that determines the onset of instability. Figure 14 shows the locus of critical points as a function of V in dimensional units for a number of values of ω and a. The plot demonstrates a substantial destabilization at small pulling speeds ($s \propto V$ is small), stabilization at moderate values of V ($s \simeq 1$), and no influence of the flow when V is large ($s \gg 1$). Both stabilization and destabilization become more pronounced as the flow amplitude a is increased at fixed frequency ω. Note the presence of cusps in the curves that correspond to shifts between different instability branches. In the case of $\mu=384.6$, which corresponds to a shear rate to pulling speed ratio of $a\omega/V=4.0\times10^2$, we observe destabilization due to the appearance of the oscillatory instability (relative to the trend observed in the stationary branch). For example, a pulling speed $V=50\,\mu\mathrm{m/s}$ falls within the range of oscillatory instability, and the corresponding amplitude and frequency of shear are $a=2.5\times10^{-3}\,\mathrm{cm}$, and $\omega=8\times10^2\,\mathrm{s}^{-1}$.

We do not have at present a clear understanding of the mechanism leading to the oscillatory instability, but we can offer a conjecture based on the structure of the neutral curves used to obtain the stability diagram discussed above. Figure 15 shows how the neutral curves $C_\infty(2\pi/\lambda)$ change as the

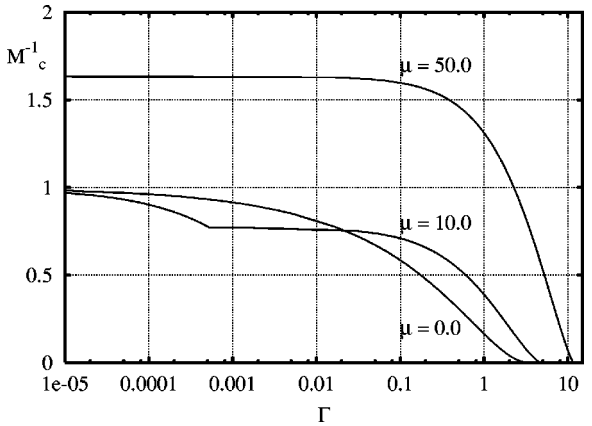

FIG. 12. Critical curves $M_c^{-1}(\Gamma)$ (from the maxima of the corresponding neutral curves) for stationary instability for $K=0.3$, $s=0.1$, and a set of values of μ.

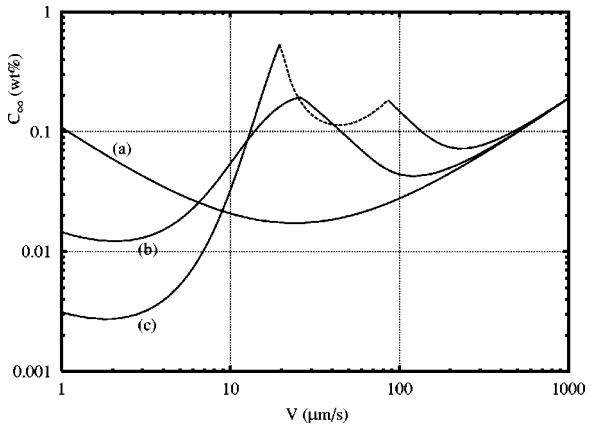

FIG. 14. Critical values of the concentration C_∞ versus pulling speed V in dimensional units for succinonitrile-acetone in a temperature gradient $G=20\,\mathrm{K/cm}$ for a number of combinations of the flow angular frequency ω and amplitude a. The solid (resp. dashed) lines mark the onset of stationary (resp. oscillatory) instability. (a) Case without flow ($\mu=0$); (b) $\omega=800.0\,\mathrm{s}^{-1}$, $a=1.0\times10^{-3}\,\mathrm{cm}$ ($\mu=61.5$), (c) $\omega=800.0\,\mathrm{s}^{-1}$, $a=2.5\times10^{-3}\,\mathrm{cm}$ ($\mu=384.6$).

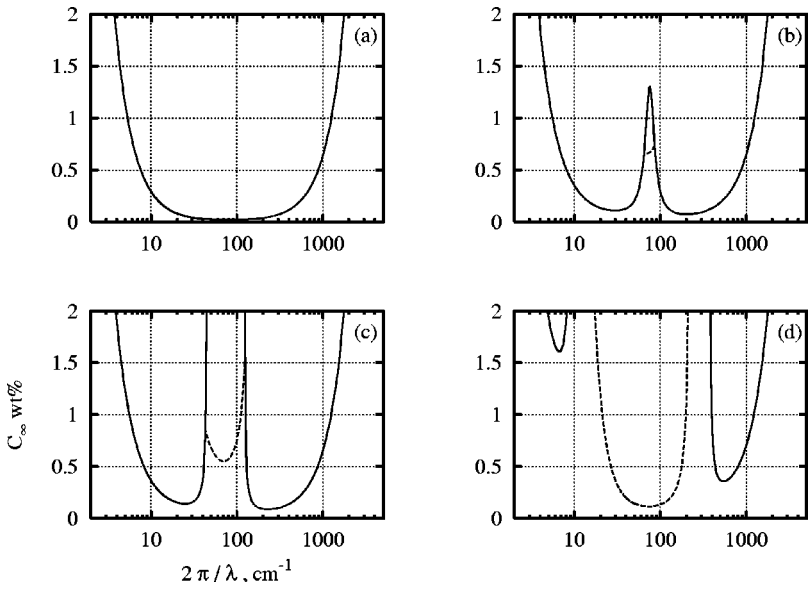

FIG. 15. Neutral curves for succinonitrile-acetone in a temperature gradient $G=20$ K/cm. The pulling speed $V=50.0\ \mu$m/s, the flow angular frequency $\omega=800.0\ \mathrm{s}^{-1}$ in cases (b), (c), and (d). The solid (resp. dashed) lines mark the onset of stationary (resp. oscillatory) instability. (a) Case without flow ($\mu=0$), (b) ($\mu=61.5$), (c) ($\mu=74.6$), (d) ($\mu=384.6$).

flow amplitude is increased. The appearance of the oscillatory branch connecting two distinct stationary branches closely resembles the case in which convective and morphological instabilities are weakly coupled.[20] The mechanism responsible for the oscillatory instability in that case was explained by Davis,[25] and it relies on qualitative differences between the eigenfunctions of the flow and concentration perturbations corresponding to convective and morphological modes of instability. The oscillatory marginal modes arise from the competition between the two. A similar mechanism is possible in our case. We do not find significant differences in the flow structure near the interface; the direction of the steady streaming ahead of the modulated front is independent of the wave number, and fluid moves from troughs to crests. However, we observe that appearance of the oscillatory instability is always accompanied by the emergence of the band of wave numbers corresponding to positive perturbation of the concentration field ahead of crest [computed from Eq. (29) linearized about the interface]. Within this range the flow progressively stabilize the system against the stationary perturbations as the flow amplitude is increased (see Fig. 15). A collateral result of this stabilization is the splitting of the stationary branch into short and long wavelength ones.

In summary, when the free-stream flow in the melt undergoes oscillatory motion parallel to the undisturbed interface, a perturbation of the solid-melt interface leads to the formation of secondary flows comprised of both oscillatory and steady components. When the amplitude of the flow oscillation away from the interface is small compared with the wavelength of the interface perturbation ($2\pi a/\lambda \ll 1$), the structure of the secondary flow can be obtained analytically as it adiabatically follows the (slow) motion on the interface, as shown in Sec. II. Mean transport terms arising from convection of the base solute distribution, and from nonlinear interaction between the base velocity field and the oscillatory part of the solute disturbance modify both the solute composition at the interface, and the solute gradient ahead of it. The slowly varying equation governing solute transport has been derived in Sec. III under assumptions that Schmidt number and dimensionless frequency are of the same order and large, $\mathrm{Sc}\propto\Omega\gg 1$. This equation along with the boundary conditions averaged over the fast time have been used in Sec. IV to obtain the neutral stability surface for a moving solid-melt interface. We find both regions of stationary and oscillatory instability. For small ratios of the viscous to solutal layer thicknesses, s, the flow generally destabilizes the planar interface. For $s\simeq 1$, the flow stabilizes the stationary branch, but it can also excite an oscillatory instability. For large s, the effect of the flow is small.

ACKNOWLEDGMENT

This research has been supported by the Microgravity Science and Applications Division of NASA under Contract No. NAG3-1885.

APPENDIX

The coefficients in Eqs. (13) and (26) are

$$A_1=-1,\quad A_2=\frac{1}{2i(i+k^2)},\quad A_3=-\frac{1}{i(2k+\alpha^*)^2},$$

$$B_1=-(A_1+A_2+A_3), \tag{A1}$$

$$B_2=(\rho-k)A_1+(\rho+\alpha^*-k)A_2+\alpha^*A_3,$$

$$E_1=\frac{1}{2i(i+k^2s^2)}-1,\quad E_2=1-\frac{1}{i(2ks+\alpha^*)^2},$$

$$F_1=-(E_1+E_2), \tag{A2}$$

$$F_2=(ks-\rho_s)+(\rho_s+\alpha^*-ks)(E_1+1)+\alpha^*(E_2-1),$$

$$
\begin{aligned}
h_0(\sigma,k,s) &= [\kappa(z;\sigma,k,s)+\kappa^*(z;\sigma^*,k,s)]\big|_{z=0},\\
g_0(\sigma,k,s) &= \frac{d}{dz}[\kappa(z;\sigma,k,s)+\kappa^*(z;\sigma^*,k,s)]\big|_{z=0},\\
\kappa(z;\sigma,k,s)\big|_{z=0} &= Q\left(\frac{E_1}{k^2+\sigma-a_1^2-a_1}+\frac{E_2}{k^2+\sigma-a_2^2-a_2}-\frac{F_1 s(k-\sigma)+F_2(1+2k)}{s(k-\sigma)^2}\right),\\
\frac{d}{dz}\kappa(z;\sigma,k,s)\big|_{z=0} &= Q\left(\frac{-(1+a_1)E_1}{k^2+\sigma-a_1^2-a_1}-\frac{(1+a_2)E_2}{k^2+\sigma-a_2^2-a_2}+(1+k)\frac{F_1 s(k-\sigma)+F_2(1+2k)}{s(k-\sigma)^2}-\frac{F_2}{s(k-\sigma)}\right),
\end{aligned}
\tag{A3}
$$

where $a_1=(\rho_s+\alpha^*)/s$, $a_2=(ks+\alpha^*)/s$ and $Q=\alpha^3/[4(\rho_s-ks)]$;

$$
\begin{aligned}
f_1(s) &= -\frac{1}{4}\frac{\sqrt{2}(-3+s^2+\sqrt{2}s)}{(s^2+\sqrt{2}s+1)(s+\sqrt{2})},\\
f_2(s) &= -\frac{1}{8}\frac{20s^6+83\sqrt{2}s^5+292s^4+300\sqrt{2}s^3+368s^2+115\sqrt{2}s+24}{(s^2+\sqrt{2}s+1)^2(s+\sqrt{2})^2},\\
f_3(s) &= -\frac{2\sqrt{2}(3s^2+4\sqrt{2}s+4}{s(s^2+2\sqrt{2}s+4)^2}.
\end{aligned}
\tag{A4}
$$

[1] W. W. Mullins and R. F. Sekerka, "Stability of a planar interface during solidification of a dilute binary alloy," J. Appl. Phys. **35**, 444 (1964).
[2] J. S. Langer, "Instabilities and pattern-formation in crystal-growth," Rev. Mod. Phys. **52**, 1 (1980).
[3] S. R. Coriell, G. B. McFadden, and R. F. Sekerka, "Cellular growth during directional solidification," Annu. Rev. Mater. Sci. **15**, 119 (1985).
[4] B. T. Murray, S. R. Coriell, A. A. Chernov, and G. B. McFadden, "The effect of oscillatory shear flow on the step banching," J. Cryst. Growth **218**, 434 (2000).
[5] M. E. Glicksman, S. R. Coriell, and G. B. McFadden, "Interaction of flows with the crystal-melt interface," Annu. Rev. Fluid Mech. **18**, 18 (1986).
[6] S. R. Coriell and R. F. Sekerka, "Effect of convective flow on morphological stability," Physicochem. Hydrodyn. **2**, 281 (1981).
[7] R. T. Delves, "Theory of the stability of a solid–liquid interface during growth from a stirred melts," J. Cryst. Growth **8**, 13 (1971).
[8] D. J. Wollkind and L. A. Segel, "A nonlinear stability analysis of the freezing of a dilute binary alloy," Philos. Trans. R. Soc. London, Ser. A **268**, 351 (1970).
[9] S. R. Coriell, G. B. McFadden, R. F. Boisvert, and R. F. Sekerka, "Effect of a forced Couette flow on coupled convective and morphological instabilities during unidirectional solidification," J. Cryst. Growth **69**, 15 (1984).
[10] A. K. Hobbs and Ph. Metzener, "Long-wave instabilities in directional solidification with remote flow," J. Cryst. Growth **112**, 539 (1991).
[11] K. Brattkus and S. H. Davis, "Flow-induced morphological instabilities: The rotating disk," J. Cryst. Growth **87**, 385 (1988).
[12] K. Brattkus and S. H. Davis, "Flow induced morphological instabilities: stagnation-point flows," J. Cryst. Growth **89**, 423 (1988).
[13] H. Schlichting, *Boundary Layer Theory*, 7th ed. (McGraw-Hill, New York, 1979).
[14] L. Bühler and S. H. Davis, "Flow-induced changes of the morphological stability in directional solidification: Localized morphologies," J. Cryst. Growth **186**, 629 (1998).
[15] Y.-J. Chen and S. H. Davis, "Directional solidification of a binary alloy into a cellular convective flow: Localized morphologies," J. Fluid Mech. **395**, 253 (1999).
[16] Y.-J. Chen and S. H. Davis, "Flow-induced patterns in directional solidification: Localized morphologies in three-dimensional flows," J. Fluid Mech. **421**, 369 (2000).
[17] T. P. Schulze and S. H. Davis, "The influence of oscillatory and steady shears on interfacial stability during directional solidification," J. Cryst. Growth **143**, 317 (1994).
[18] T. P. Schulze and S. H. Davis, "Shear stabilization of morphological instability during directional solidification," J. Cryst. Growth **149**, 253 (1995).
[19] T. P. Schulze and S. H. Davis, "Shear stabilization of a solidifying front: Weakly nonlinear analysis in a long-wave limit," Phys. Fluids **8**, 2319 (1996).
[20] S. R. Coriell, M. R. Cordes, W. J. Boettinger, and R. F. Sekerka, "Convective and interfacial instabilities during directional solidification of a binary alloy," J. Cryst. Growth **49**, 13 (1980).
[21] W. H. Lyne, "Unsteady viscous flow over a wavy wall," J. Fluid Mech. **50**, 33 (1971).
[22] D. Volfson and J. Viñals, "Flow induced by a randomly vibrating boundary," J. Fluid Mech. **432**, 387 (2001).
[23] A. A. Wheeler, G. B. McFadden, B. T. Murray, and S. R. Coriell, "Convective stability in the Rayleigh–Bénard and directional solidification problems: High frequency gravity modulation," Phys. Fluids A **3**, 2847 (1991).
[24] Material parameters may be found in Ref. 18.
[25] S. H. Davis, "Hydrodynamic interactions in directional solidification," J. Fluid Mech. **212**, 241 (1990).